



# Influence of wall-to-floor connections and pounding on pre- and post-diction simulations of a masonry building aggregate tested on a shaking table

N. Bianchini<sup>1</sup> · M. P. Ciocci<sup>1</sup> · F. Solarino<sup>1</sup> · A. Romanazzi<sup>1</sup> · R. Ramirez<sup>1</sup> · J. D'Anna<sup>1</sup> · A. Aşıkoglu<sup>1</sup>

Received: 12 May 2022 / Accepted: 31 January 2023  
© The Author(s) 2023

## Abstract

This paper presents numerical simulations within the frame of the project SERA—AIMS (Seismic Testing of Adjacent Interacting Masonry Structures). The study includes blind pre-diction and post-diction stages. The former was developed before performing the shaking table tests at the laboratory facilities of LNEC (Lisbon), while the latter was carried out once the test results were known. For both, three-dimensional finite element models were prepared following a macro-modelling approach. The structure consisted of a half-scaled masonry aggregate composed by two units with different floor levels. Material properties used for the pre-diction model were based on preliminary tests previously provided to the participants. The masonry constitutive model used for the pre-diction study reproduced classical stress–strain envelope, whereas a more refined model was adopted for the post-diction. After eigenvalue analysis, incremental nonlinear time history analysis was performed under a unique sequence based on the given load protocol to account for damage accumulation. In the post-diction, the numerical model was calibrated on the data recorded during the shaking table tests and nonlinear dynamic analysis repeated under the recorded accelerogram sequence. The interaction between the two units was simulated through interface elements. Moreover, the timber floors were accounted following different strategies: not modelling or considering nonlinear wall-to-floor connections. Advantages and disadvantages are then analysed, comparing the pre-diction and post-diction results with the experimental data. Numerical results differ from the experimental outcomes regarding displacements and interface pounding, although a clear improvement is visible in the post-diction model.

**Keywords** Buildings interaction · Pounding · Wall-to-floor connection · Incremental dynamic analysis · Nonlinear time history analysis finite element modelling · Stone masonry aggregate

---

✉ N. Bianchini  
nicoletta.bianchini@gmail.com  
https://www.isise.net

<sup>1</sup> Department of Civil Engineering, ISISE, University of Minho, Guimarães, Portugal

# 1 Introduction

Ancient unreinforced masonry (URM) buildings are often composed of masonry walls with timber floors and roofs. In European city centres, they have been typically constructed in continuity one to each other over centuries, resulting in complex aggregates of adjacent URM buildings (i.e. structural units) with a large variety of geometries, materials and construction techniques (Giuffr  1993; Carocci 2012). Despite the formidable inventory of these buildings, they present some common features that make them highly vulnerable to earthquakes. Such features include, but are not limited to, the low masonry tensile strength and the poor connection between structural elements—namely wall-to-floor (WF), wall-to-wall (WW) and unit-to-unit (UU) connections—and the low in-plane stiffness of timber floors (Bruneau 1994; Miha Tomaževič 1999; Lourenço et al. 2011; Solarino et al. 2019). As a result, out-of-plane (OOP) failures of masonry walls typically occur in URM buildings and aggregate, as confirmed in past earthquakes observations (D’Ayala and Paganoni 2011; Dizhur et al. 2011; Penna et al. 2014; Sorrentino et al. 2019; Stepinac et al. 2021) and previous experimental tests carried out at building level (Tomaževič et al. 1991; Tomaževič 1992; Benedetti et al. 1998; Mazzon et al. 2010; Senaldi et al. 2014; Vintzileou et al. 2015).

Among different numerical methods, nonlinear analysis on finite element (FE) models using macro-modelling approach is widely used for the seismic assessment of historical masonry buildings (Lourenço 2002; Roca et al. 2010; D’Altri et al. 2019). However, there are several critical questions which arise when simulating the behaviour of such buildings, such as the choice of proper modelling assumptions (Angelillo 2014; Saloustros et al. 2020; Ciocci et al. 2018;  lvarez et al. 2019). In this regard, the accurate simulation of structural connections and timber floors represents a major challenge, as also evidenced by recent numerical studies (D’Altri et al. 2018; Castellazzi et al. 2018; Ařıkođlu et al. 2020; Parisse et al. 2021; Puncello et al. 2022).

For the connections between structural elements, common choices involve simplifications in current practice, as their construction details are typically unknown and limited experimental data on their structural behaviour are currently available. In most cases, they are simulated as perfect connection/disconnection depending on the quality of existing links, while the real condition provided is somewhat in between. Timber floors are typically neglected or modelled assuming linear elastic behaviour. The first approach is typically adopted when the efficiency of WF connections is assumed to be so weak to disrupt the continuous transfer of loads to the rest of the structure. The second assumption is corroborated by the fact that no significant damage in timber floor prior to the failure of WF connection is typically observed. Consequently, the definition of a proper nonlinear behaviour of WF connections is fundamental for an accurate numerical prediction of URM seismic response.

This paper presents a numerical study carried out for the pre- and post-diction competitions organised within the SERA—AIMS project (Tomić et al. 2022a, b). The study aims at simulating the behaviour of a half-scale stone masonry aggregate, subjected to shaking table testing at LNEC facilities. Section 2 describes the pre-diction finite element (FE) models in terms of geometry, morphology, connections and support conditions. Two FE models are considered in the blind prediction, namely FEM-4 and FEM-5. They differ in the modelling strategy adopted for the timber floors: FEM-4 implements timber beams with nonlinear WF connections, while FEM-5 does not model timber floors. The results obtained by performing incremental dynamic analysis on the two pre-diction models are

then compared in Sect. 3, with regard to the shaking table results. Based on the additional information provided by the experimental tests, an updated model is put forward for the post-diction study, i.e. FEM-PS-5 (Sect. 4). In Sect. 5, the results obtained from FEM-PS-5 are discussed quantitatively (base shear forces and displacements) and qualitatively (crack pattern), and then compared with the shaking table testing results.

## 2 Description of the pre-diction models: FEM-4, FEM-5

The case study is a  $4.95 \times 2.50$  m<sup>2</sup> half-scale test specimen of a two-unit masonry aggregate constructed with double-leaf irregular stone masonry walls, timber floors simply supported on the walls, and dry connection between the units. The wall thickness of the masonry aggregate ranges between 35 and 25 cm, and 15-cm-thick spandrels are beneath the openings. As shown in Fig. 1, the two units differ for number of storeys, interstorey height and beam orientation. Further details about the aggregate test specimen can be found in Tomić et al. (2022a, b).

The models used in the pre-diction study, namely FEM-4 and FEM-5, are built in GiD+OpenSees (Papanikolaou et al. 2017), which allows pre- and post-processing of the numerical results, and a macro-modelling approach is adopted in OpenSees v.3.0.3 (McKenna et al. 2000). The two models consider the same modelling assumptions, except for timber floors. As mentioned by Tomić et al. (2022a, b), the timber beams are simply supported on the masonry walls representative of a rather weak WF connection.

Therefore, two different modelling strategies are adopted: FEM-4 implements timber beams which are connected to the walls by means of a hysteretic uniaxial model that is calibrated on the experimental data obtained by Moreira 2015 on poor WF connections (Fig. 2a), while FEM-5 does not model the timber floors (Fig. 2b).

For the specific case study, the interaction between the structure and the shake table is neglected; therefore, fixed based boundary conditions are assumed at the foundation.

The numerical models adopt the same geometry of the test specimen aggregate at 1:2 reduced scale, according to Tomić et al. (2022a, b). Masonry walls and timber lintels

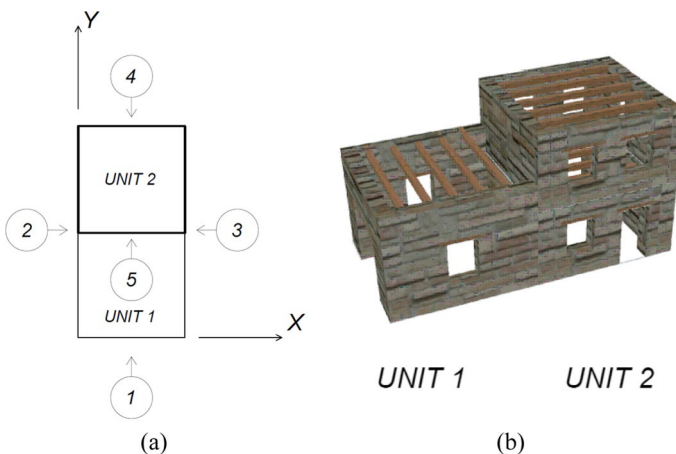


**Fig. 1** Stone masonry aggregate test specimen adopted in the experimental campaign carried out by Tomić et al. (2022a, b): **a** floor plan; **b** 3D view

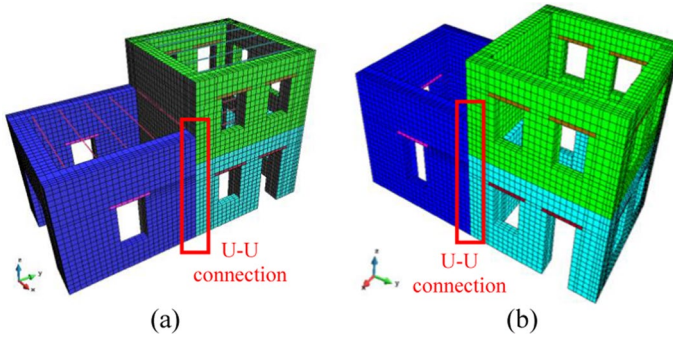


**Fig. 2.** 3D views of the structured mesh of the models submitted to the SERA—AIMS blind prediction competition: **a** FEM-4 w/ beams; **b** FEM-5 w/o beams

are modelled through 8-node *StBrick* (Love and Sandia National Laboratories 2018) elements, using a structured mesh with characteristic length of 5 or 10 cm: in this way, a minimum of three nodes is guaranteed along the thickness of the masonry walls. The constitutive material model used for masonry is based on Faria et al. (1998), which reproduces the classical stress–strain envelopes, strength enhancement for confinement, and residual compression strain upon load reversals (Fig. 3). As the adopted material model does not allow for the definition of density, masonry masses are distributed on each element node according to the element size. The material properties adopted for masonry are summarised in Table 1. The tensile and compressive strengths are assumed based on the vertical and diagonal compression tests carried out by Guerrini et al. (2017, 2019) and Senaldi et al. (2018).

To define the required damage parameters and the plastic deformation, preliminary numerical analyses were carried out simulating the in-plane shear tests which were performed within the same experimental program (Senaldi et al. 2018). These analyses also allowed to calibrate the Young’s modulus of masonry, resulting in a value of 2.0 GPa. The indexes reported in Table 1 take into account the response in terms of damage and plasticity under “loading”, “unloading” and “reloading” actions, and can range from fully damage response to fully plastic behavior. In this way, it is possible to calibrate

**Fig. 3** Plastic-damage material constitutive model adopted for masonry (Faria et al. 1998)

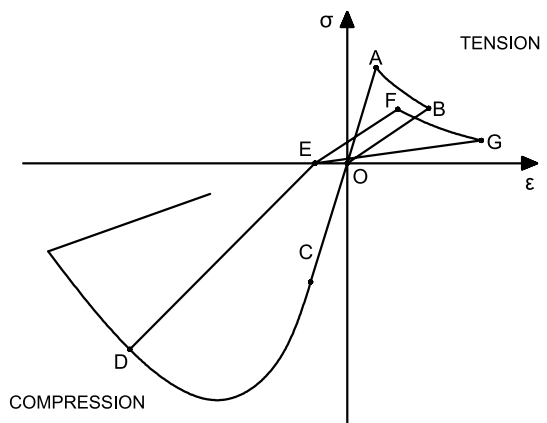


**Table 1** Material properties adopted for masonry and timber in the pre-diction numerical model

	Masonry properties	Timber
Young’s modulus $E$ [MPa]	2000.0	10,000.0
Poisson’s ratio $\nu$ [-]	0.14*	0.30
Density [kg/m <sup>3</sup> ]	1980*	410.0
Compressive strength $f_c$ [MPa]	1.30*	
Tensile strength $f_t$ [MPa]	0.17*	
Damage parameter in compression $A_n$ [-]	2.0	
Damage parameter in compression $B_n$ [-]	0.7	
Damage parameter in tension $A_p$ [-]	1.0	
Plastic deformation coefficient $\beta$ [-]	0.4	

\*Value provided from the experimental characterisation tests

the energy dissipation due to hysteresis. As regards the plastic deformation coefficient, it indicates whether the material model considers plastic or solely elastic-damage effects (Faria et al. 1998).

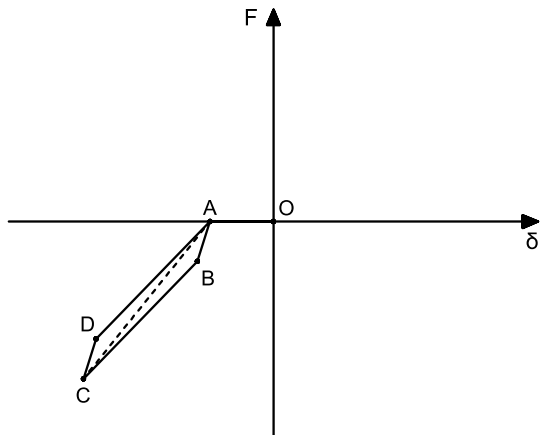
With regard to the timber beams modelled in FEM-4, linear elastic isotropic behaviour is assumed. The mean values of density and Young’s modulus parallel to the grain are adopted according to UNI EN 338 (2016), assuming a timber class C22.

The UU connection, which interests the contact between Unit 1 and Unit 2, is modelled as a 3D interface by means of *zeroLengthImpact3D* elements (Arash et al. 2014). The adopted material model is based on simplified Hertz impact theory and Coulomb friction theory, allowing to reproduce pounding/impact and friction interaction at the interface. The response of the adopted impact material model is presented in Table 2 and Fig. 4. The energy dissipated during an impact is function of  $K_h$ , which represents the impact stiffness parameter, and the maximum penetration ( $\delta_m$ ) during the pounding event. The  $\delta_m$  value is

**Table 2** UU connection properties

$K_h$ [Nm <sup>-3/2</sup> ]	$\delta_m$ [mm]	$\delta_y$ [mm]	$\mu$ [-]	$c$ [MPa]
1e+09	10.0	1.0	0.6	0.0

**Fig. 4** Response of impact material model used for the UU connection



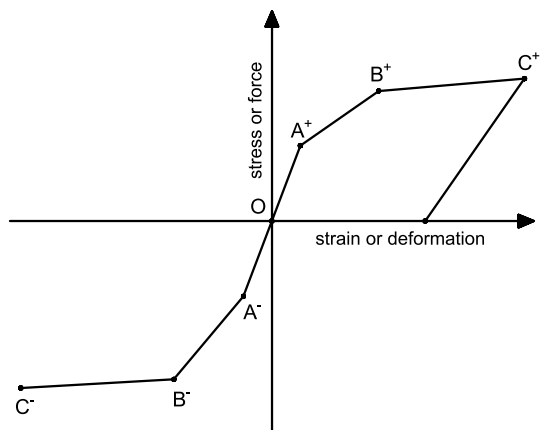
assumed as 10 mm and defines the yield parameter of the material as  $\delta_y = 0.1 \times \delta_m$ . The friction coefficient ( $\mu$ ) and the cohesion ( $c$ ) values are assumed of 0.6 and 0.0 MPa, respectively, as suggested in literature (Vasconcelos et al. 2008; Lourenço and Ramos 2004; Casapulla and Portioli 2016). A good connection is assumed between the orthogonal walls of the aggregate (Tomić et al. 2022a, b); therefore, the WW connection is modelled as a continuum between the masonry solid elements.

As mentioned above, the FE models implement two different modelling strategies to simulate the timber floors weakly connected to the walls. In FEM-4, *truss* elements with linear elastic isotropic behaviour are used to model the timber beams. The WF connection is simulated as a single axial spring-like element by means of *zeroLengthElement* (Fenves 2014) with nonlinear behaviour (Table 3 and Fig. 5). The adopted hysteretic material model allows for pinching and cyclic degradation (Scott and Filippou 2016). The input parameters are calibrated according to the experimental pull-out tests performed by Moreira 2015. These tests were carried out on unstrengthened WF connections, reasonably representing the configuration adopted by Tomić et al. (2022a, b). More details on the calibration of the axial hysteretic law adopted for WF connections can be found in Solarino et al. (2021). In

**Table 3** Hysteretic material properties set for WF connections

Description	Symbol	Value
Envelope points in the positive direction	$A^+, B^+, C^+$	$A^+ = (0.4 \text{ mm}; 4.0 \text{ kN})$ $B^+ = (40.0 \text{ mm}; 4.1 \text{ kN})$ $C^+ = (42.0 \text{ mm}; 0.4 \text{ kN})$
Envelope points in the negative direction	$A^-, B^-, C^-$	$A^- = (5.0 \text{ mm}; 100.0 \text{ kN})$ $B^- = (10.0 \text{ mm}; 200.0 \text{ kN})$ $C^- = (20.0 \text{ mm}; 300.0 \text{ kN})$
Pinching factor for deformation during reloading	pinchX	0.75
Pinching factor for force during reloading	pinchY	0.1
Damage due to ductility	D1	0.0
Damage due to energy	D2	0.0
Power used to determine the degraded unloading stiffness based on ductility	$\beta$	0.0

**Fig. 5** Hysteretic material model used for WF connections



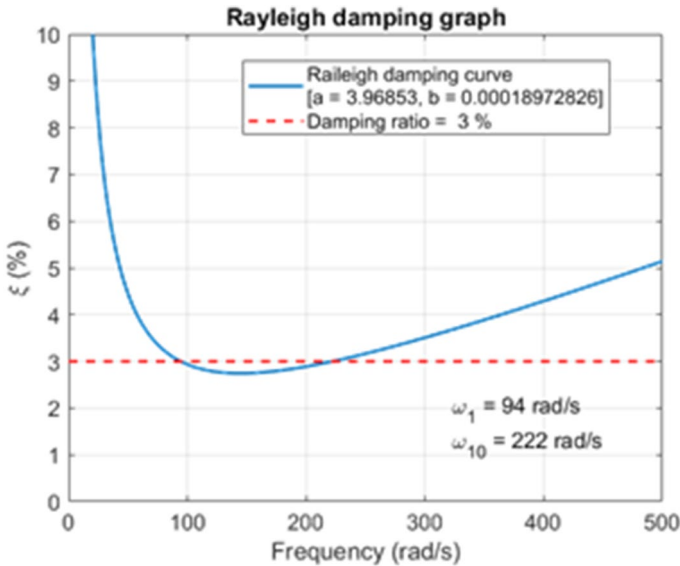


**Fig. 6** Rayleigh damping coefficient distribution and frequency bandwidth

FEM-5, the timber floors are not modelled, and the tributary floor masses are assigned to the corresponding nodes of the masonry walls.

### 3 Pre-diction: analysis and results

Models FEM-4 and FEM-5 are utilised for the blind pre-diction challenge performing non-linear dynamic analyses with time integration. To introduce additional damping due to non-linear phenomena, the viscous damping matrix  $\mathbf{C}$  is assumed using Rayleigh formulation as a linear combination of the mass  $\mathbf{M}$  and the stiffness  $\mathbf{K}$  matrices, i.e.  $\mathbf{C} = \alpha_M \mathbf{M} + \beta_K \mathbf{K}$  (Chopra 2012). It is worth to mention that a current stiffness matrix approach is used, and hence damping matrix updates when the tangent stiffness changes (Charney 2008). The mass and stiffness proportional damping constants,  $\alpha_M$  and  $\beta_K$ , are calculated with a value of 3.96853 and 0.0001897 respectively (Fig. 6). These values are estimated considering a damping ratio  $\xi$  of 3%, and the first ten modal frequencies which excite around the 70% of the cumulative participation masses in X and Y directions. The value of damping ratio is assumed based on previous numerical studies on existing masonry buildings (e.g. Mendes and Lourenço 2014; Parisse et al. 2021). It is worth noting that for model FEM-4 the eigenvalue analysis is performed by neglecting floor trusses in order to evaluate a wider range of reasonable global modes. As a result, the first natural frequency is about 15 Hz for both numerical models.

The nonlinear dynamic analysis is performed based on the Hilber-Hughes-Taylor (HHT) time integration method (Hilber et al. 1977), also known as the  $\alpha$ -method. Being an extended version of the Newmark method, in the HHT method a further numerical damping can be introduced. This allows to deal with the noise caused by the abrupt change in masonry from an elastic to fully cracked state with zero stiffness variation. HHT method is used adopting a  $\alpha$  value of 0.9, calculated on the basis of  $\alpha = \alpha_{HHT} + 1$  where  $\alpha_{HHT}$  is

assumed to be  $-0.1$  according to the literature (Mendes and Lourenço 2010). As concerns the time step,  $\Delta_t$  is defined as  $0.003536$  s, taking into account the requirements arising from the total duration of the analysis, the lowest frequency obtained for the numerical model (Mendes and Lourenço 2010), as well as the Cauchy-Froude similitude law related to the half-scale factor of the test specimen (Carvalho 1998).

In the pre-diction analysis, the two horizontal components of the 1979 Montenegro earthquake Albatros station records are used as seismic input in the numerical analysis. It is noted that, the time reflects the similitude law due to the reduced scale of the test specimen. To simulate the incremental dynamic test and the consequent damage accumulation, the seismic signals of the entire experimental sequence are applied as a single ground motion. This choice requires a new set of filters and baseline correction, which are properly implemented in the incremental dynamic analysis (IDA). As preliminary transient analyses showed no significant influence of the 25% and 50% test sequences (Runs 1.1–1.3 and Runs 2.1–2.3), the incremental loading sequences shown in Table 4 are applied to the numerical models. Therefore, the total duration of the performed IDA analyses is  $352.4$  s for FEM-4 and  $235.4$  s for FEM-5 (Fig. 7).

The numerical pre-diction results are investigated in terms of maximum absolute value of base shear forces (BS<sub>x</sub>, BS<sub>y</sub>), roof displacements (Rd2–Rd3) and interface openings (Id3–Id4). The selected quantities are presented in Fig. 8. Figure 9 compares the results obtained for FEM-4 and FEM-5, per each run. Base shear forces clearly reflect the main direction of the earthquake and increase with increasing PGA level. A similar response in terms of base shear and displacements is observed at Run 3.1 for both models, also confirming the negligible influence of the previous discarded runs for FEM-5 (i.e. Runs 2.1–2.3). At Run 3.1, the maximum absolute value of BS<sub>y</sub> is  $143$  kN and  $139$  kN for FEM-4 and FEM-5, respectively. After Run 3.3, FEM-5 undergoes about two times higher values for roof displacements and interface opening when compared to FEM-4. At the end of the entire loading sequence (Run 4.3), FEM-4 presents a maximum Rd2 value of  $35$  mm, while FEM-5 registers about  $56$  mm. This is probably due to the presence of WF connections in FEM-4 that counteracts the separation of opposite walls. Indeed, the maximum wall-to-floor slip attained at second floor of Unit 2 solely

**Table 4** Nominal SERA AIMS shake-table testing sequence and runs adopted in the pre-diction numerical models

Run id	Direction	Level of shake	Nominal PGA	FEM-4	FEM-5
1.1	Y	25.0%	0.219 g	Discarded	Discarded
1.2	X	25.0%	0.156 g	Discarded	Discarded
1.3	X,Y	25.0%	0.219 (y)/0.156 (x) g	Discarded	Discarded
2.1	Y	50.0%	0.438 g	✓	Discarded
2.2	X	50.0%	0.313 g	✓	Discarded
2.3	X,Y	50.0%	0.438 (y)/0.313 (x) g	✓	Discarded
3.1	Y	75.0%	0.656 g	✓	✓
3.2	X	75.0%	0.469 g	✓	✓
3.3	X,Y	75.0%	0.656 (y)/0.469 (x) g	✓	✓
4.1	Y	100.0%	0.875 g	✓	✓
4.2	X	100.0%	0.625 g	✓	✓
4.3	X,Y	100.0%	0.875 (y)/0.469 (x) g	✓	✓



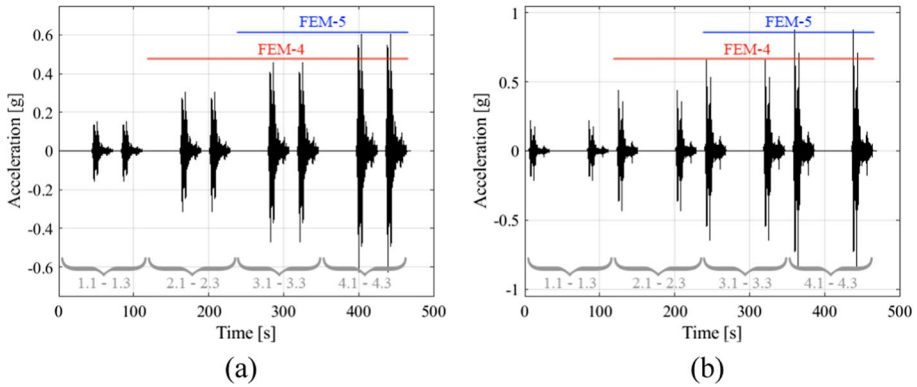
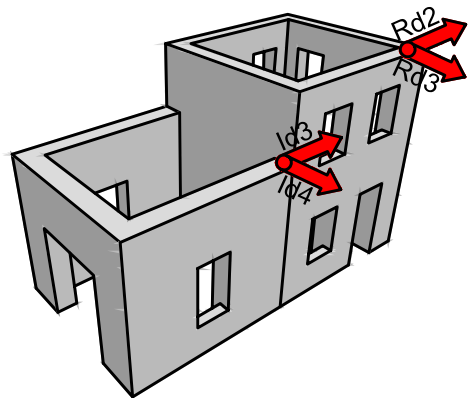


**Fig. 7** Acceleration time histories of the Montenegro 1979 earthquake recorded at the Albatros station applied to the pre-diction numerical models: **a** X-direction; **b** Y-direction

**Fig. 8** Compared quantities for the blind pre-diction study



corresponds to 2% of the total displacement capacity of the connection, far enough from the failure. This is due to the fact that the WF connections implemented in FEM-4 remain in the elastic range. Hence, the OOP mechanism of the façade is counteracted by the timber beams in FEM-4, leading to a lower Rd2 value when compared to FEM-5.

As mentioned in Tomić et al. (2022a, b), the nominal spectra and PGA of Run 3.1 are rather close to the effective spectra and PGA of Run 2.1. For this reason, the response predicted by FEM-4 and FEM-5 for Run 3.1 is compared to the experimental results of Run 2.1. Figure 10 shows the comparison in terms of the selected results. It is noted that the numerical and experimental results are plotted removing the offsets due to the previous runs. The shape of the numerical displacement time histories matches rather well with the measured results, suggesting a good estimation of the damping parameters and no vibratory response (Panella et al. 2017). It is to be noted that the experimental and numerical maximum displacements occur at similar time. However, these values are significantly underestimated by the numerical models, as also the UU interface openings. This might also be attributed to the additional three runs at 12.5% (i.e. Runs 0.1–0.3) which were actually added at the experimental testing phase (Tomić et al. 2022a, b). In

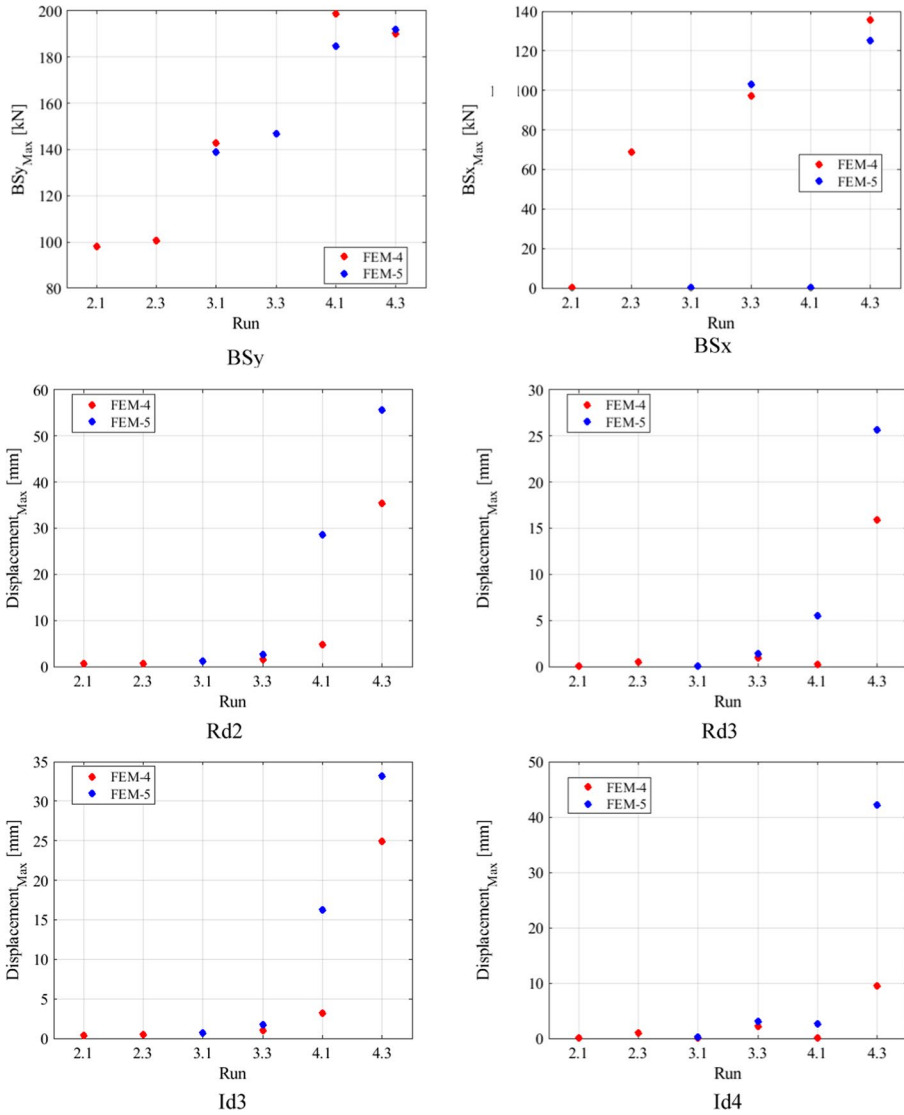


**Fig. 9** Comparison between the numerical results obtained from FEM-4 and FEM-5: maximum absolute values of base shear forces, displacements and interface openings

terms of base shear, FEM-4 predicts the maximum and minimum BSy values with an error of 30% and 13% respectively, while FEM-5 has an error of 27% and 18%.

The crack pattern predicted by the numerical models is presented through principal tensile strains, being a good damage index according to Mendes and Lourenco (2010). It is noted that the tensile strains shown in Fig. 11 correspond to a specific time step, i.e. when the maximum base shear value is obtained for FEM-4 and FEM-5. When compared to FEM-5, FEM-4 shows OOP overturning mechanisms that are counteracted, since the WF connections remain in the linear elastic range.

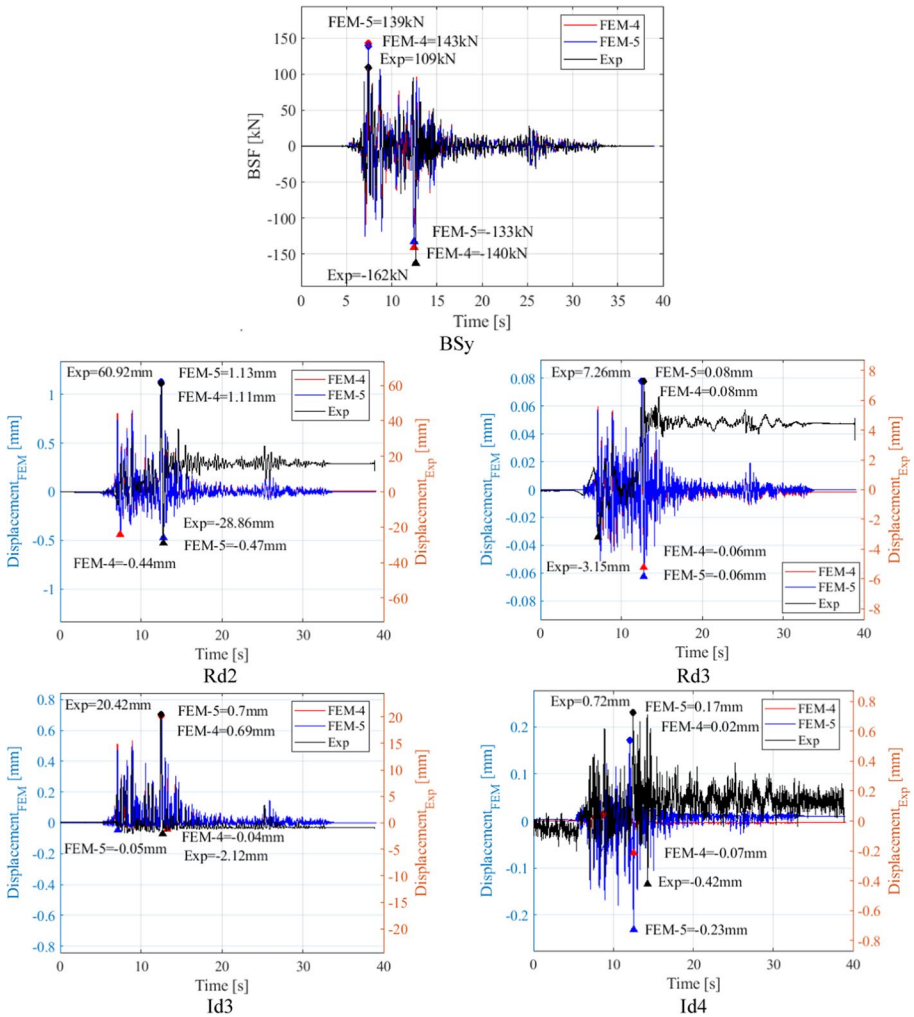


**Fig. 10** Comparison between the experimental results (Run 2.1) and numerical results (Run 3.1): base shear, displacement and interface opening time histories

When comparing with the experimental observations, both models correctly predict less cracking in Unit 1 with respect to Unit 2. In Unit 2, cracking is observed close to the opening of Façades 2 and 3 for both models, being more significant in FEM-5. FEM-4 predicts shear cracking while the behaviour observed experimentally is purely flexural. Though with less crack propagation, FEM-5 correctly predicts the flexural mechanism in the upper storey of Facades 2 and 3. In addition, FEM-5 captures the horizontal cracking at the base of Façade 5, as well as the pounding interacting between the two units. The experimental evidences show an OOP mechanism for Façade 4, which involves also the transversal walls and Façade 5. Although the development of this mechanism is reproduced in FEM-4, the displacements are restricted by the presence of the floor beams. On the other hand, the OOP mechanism of Façade 4 is fully developed in FEM-5, yet not involving the rest of the structure as in the experimental observations.

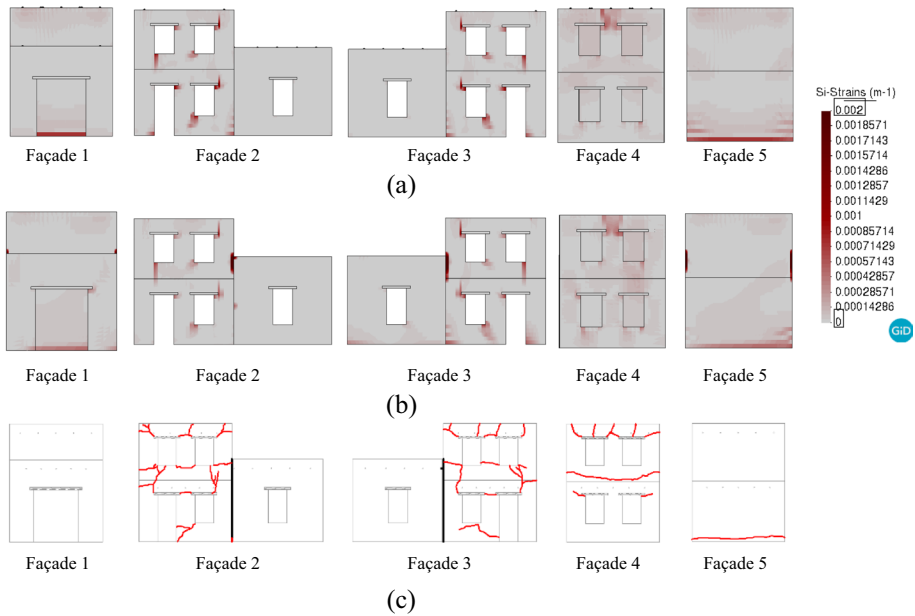


**Fig. 11** Comparison between the numerical results in terms of crack pattern: **a** FEM-4 for Run 3.1; **b** FEM-5 for Run 3.1; **c** the experimental results for Run 2.1

#### 4 Description of the post-diction model: FEM-PS-5

Based on the pre-diction investigations and the shaking table results, the assumption of neglecting timber floors seems to be more suitable for simulating the observed experimental response. Thus, the numerical model without beams is selected to carry out the post-diction study. The information gained from the experimental tests are then used to improve the numerical simulation, and the model is updated into FEM-PS-5. The modifications carried out between the pre-diction and post-diction phases are summarised in Fig. 12.

Still adopting a macro-modelling approach in OpenSees software (McKenna et al. 2000), FEM-PS-5 is constructed in STKO graphical interface for pre- and post-processing (Petraçca et al. 2017a), allowing to implement a further refined damage model for masonry, i.e. Damage TC3D. Being based on the work carried out by Faria et al. (1998), this model put forward by Petraçca et al. (2017a, b) and Petraçca and Camata (2019) allows to account for residual plastic strains due to damage both in compression and tension, as shown in Fig. 13. In addition, it permits to implement a mixed IMPLicit-EXplicit integration scheme (IMPL-EX), being more stable and effective in case of masonry structures.

Another important update adopted in FEM-PS-5 concerns the Young's modulus value for masonry. As mentioned by Tomić, Penna and Dejong (2022a, b), the first fundamental frequency obtained experimentally for the undamaged structure is approximately 7.7 Hz, corresponding to a fundamental period of 0.13 s. As the experimental information is limited only to the first natural frequency of the aggregate structure, this value is then adopted as target frequency while performing the model updating on

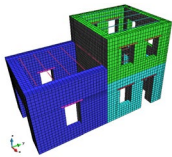
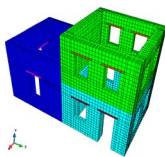
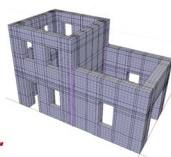
	Pre-diction		Post-diction
			
	FEM-4	FEM-5	FEM-PS-5
<b>Masonry</b>	(Faria, Oliver, and Cervera 1998)		(Petracca et al. 2017; Petracca and Camata 2019)
Material Model	E = 2000 MPa		E = 690 MPa
Main parameters	$f_c = 1.30$ MPa		$f_c = 0.69$ MPa
	$f_t = 0.17$ MPa		$f_t = 0.07$ MPa
<b>Timber floors</b>	Truss elements		Not modelled
Beams	Nonlinear behaviour		N/A
WF connections	Not modelled		Not modelled
	N/A		N/A
<b>UU connection</b>	Simplified Hertz impact theory and Coulomb friction theory		
Material Model	$\delta_{max} = 10$ mm		$\delta_{max} = 20$ mm
Main parameters	c = 0.0 MPa		
	$\mu = 0.6$		
	$K_h = 1e9$ Nm <sup>-3/2</sup>		
<b>Damping</b>	Rayleigh damping model, $\xi = 3\%$		
<b>Seismic input</b>	Nominal shake-table testing sequence		Actual shake-table testing sequence

Fig. 12 Comparison between the pre- and post-diction models

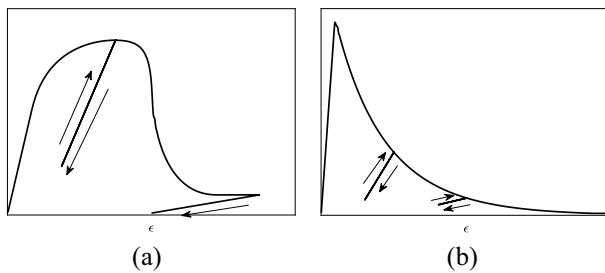


Fig. 13 Damage TC3D material model used for masonry: **a** compressive cyclic behaviour; **b** tension cyclic behaviour (Petracca et al. 2017a, b)

FEM-PS-5 with the aim to calibrate elastic material properties. However, matching the natural frequency obtained experimentally results in adopting a significant low value of E for masonry. With the aim to keep the Young’s modulus value of masonry in a reasonable range, the lower bound limit value that is suggested by the Italian code (Ministero delle Infrastrutture e Trasporti 2019) for same masonry typology is adopted in FEM-PS-5, i.e. E = 690MPa (Fig. 12). It is noted that, when adopting this E value, the first frequency obtained numerically is about 9.9 Hz, significantly lower than the value obtained in the pre-diction phase (15 Hz). Thus, the error drops from 92% (FEM-5) to 28% (FEM-PS-5) when compared to the experimental frequency.

Reflecting the decrease in the Young's modulus value of masonry, a lower value of compressive strength is assumed in FEM-PS-5. The compressive strength  $f_c$  is equal to 0.69 MPa, calculated using the relation  $f_c = E/\alpha$  by assuming a value of  $\alpha = 1000$ , as suggested in Eurocode 6 (CEN 2001), and a value of  $E$  equal to 690 MPa. Accordingly, also the tensile strength  $f_t$  is decreased to a value of 0.07 MPa, as reported in Fig. 12, adopting the relation  $f_t = 0.1 \times f_c$  also suggested in Eurocode 6 (CEN 2001). As regards the other material parameters required for the Damage TC3D material model, the values are evaluated according to literature (Angelillo 2014).

Based on the information obtained experimentally, the impact behaviour for pounding of UU connections was also calibrated in FEM-PS-5. As shown in Fig. 10, the relative displacement  $Id_3$  reaches a maximum value of 20 mm, corresponding to the maximum value of impact at the level of the U-U connection. This aspect is considered to update the  $\delta_m$  value, as shown in Fig. 12. As regards the parameters to simulate the UU connection behaviour in shear, the assumptions made in the pre-diction study are kept (Fig. 12).

Following the same methodology adopted for FEM-5, nonlinear incremental dynamic analysis is performed on FEM-PS-5 for the post-diction. For the Rayleigh damping model, the  $\alpha_M$  and  $\beta_K$  constants are updated by performing eigenvalue analysis on FEM-PS-5, and keeping  $\xi = 3\%$  as it results to be a reasonable value based on the blind pre-diction results. As a consequence,  $\alpha_M = 2.99521$  and  $\beta_K = 0.000189885$  are set in FEM-PS-5.

## 5 Post-diction: analysis and results

As mentioned by Tomić et al. (2022a, b), the actual testing sequence differs from the original plan. Hence, the actual testing sequence is adopted as seismic input in the post-diction numerical analysis. Implementing the recorded input, no need of scaling the time step is required for the post-diction. Therefore, the  $\Delta_t$  adopted for the HHT method is set equal to the time step of the applied input, i.e.  $\Delta_t = 0.005$  s. As a major influence of the seismic excitation in Y-direction is observed experimentally, the analysis considers the runs with the excitation applied in this direction, namely: Runs 0.1, 0.3, 1.1, 1.3 and 2.1 (Table 5 and Fig. 14). Similarly, to the pre-diction analysis, the excitations are applied at the base of the model as a unique input, to take into account the accumulation of damage during time. As follows, the total duration of the post-diction IDA analysis is equal to 195 s.

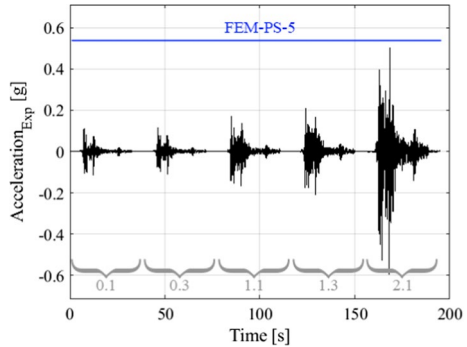
The post-diction results are again investigated in terms of maximum absolute values per each run (Fig. 15a), as well as in terms of displacements time histories at the Run 2.1 (Fig. 15b). The selected quantities are the base shear force in Y-direction (BSy), roof displacement (Rd2) and interface opening ( $Id_3$ ). As it is possible to observe in Fig. 15a, the

**Table 5** List of experimental runs evaluated in the post-diction numerical analysis on FEM-PS-5

Run notation	Direction	Level of shaking	Effective PGA*
0.1	Y	12.5%	0.113 g
0.3	Y	12.5%	0.113 g
1.1	Y	25.0%	0.170 g
1.3	Y	25.0%	0.208 g
2.1	Y	50.0%	0.593 g

\*Measured during the shaking table tests

**Fig. 14** Actual acceleration time histories applied in the post-diction numerical analysis on FEM-PS-5



numerical model reflects rather well the behaviour observed experimentally being characterised by two main responses: an almost linear trend between Run 0.1 and Run 1.3, and a nonlinear behaviour at Run 2.1. The latter is due to the occurrence of several cracks in the masonry walls that concur to reduce the stiffness of the structure induced by the high excitation at this run.

At the end of the entire loading sequence (Run 2.1), FEM-PS-5 predicts maximum BSy values of 148 kN and 127 kN in the positive and negative direction, being not significantly different from the values obtained in the pre-diction phase. When compared to the experimental results (Fig. 15b), the BSy error is 36% and 22% respectively. A general improvement in terms of displacements is observed for FEM-PS-5, with Rd2 and Id3 values which are respectively about 16 and 11 times those obtained in the blind pre-diction. This is mainly due to the updated Young's modulus adopted for masonry (Sect. 4). In comparison with the experimental results, the maximum displacements occur at similar time though a significant underestimation is still observed. However, the pounding behaviour simulated by the UU-connection in the post-diction accurately estimates the experimental results. In addition, the residual displacement Rd2 (from  $t = 15$  s until the end) is depicted in the numerical model.

As in the pre-diction study, the damage that occurs numerically is investigated from the qualitative point of view through principal tensile strains. Figure 16 presents the results at the time step when the maximum BSy value is obtained in Run 2.1 (i.e.  $t = 168.2$  s of the entire loading sequence). Overall, a considerable improvement also in terms of crack pattern is obtained for FEM-PS-5 when compared to FEM-5. Indeed, for Facades 2 and 3, the crack pattern is rather well attained by the numerical model, reflecting the observed damage in spandrels and piers: FEM-PS-5 captures the horizontal cracks of the piers at the 2nd storey as well as the flexural mechanism occurring in the spandrels at both levels. The OOP mechanism observed at the 2nd storey of Façade 4 is also numerically detected, though with some differences: in the experimental test the horizontal crack is located at the floor level, while in FEM-PS-5 it occurs between the openings at the 2nd storey. Still, the cracks at the spandrels in the upper part of Façade 4 are similar to the experimental observations. Also the OOP mechanism that occurs in Façade 5 is captured by FEM-PS-5, as well as the horizontal cracking at the base. However, a more extensive cracking is observed numerically in the upper part of this wall, with a horizontal through-wall crack at level of the interaction with Unit 1. In addition, signs of impact are also visible at the UU connection, as also detected experimentally. In particular, crushing due to pounding is observed in façade 5 at the level of the roof of Unit 1 and at the second level of Unit 2 (internal elevation in Fig. 16).

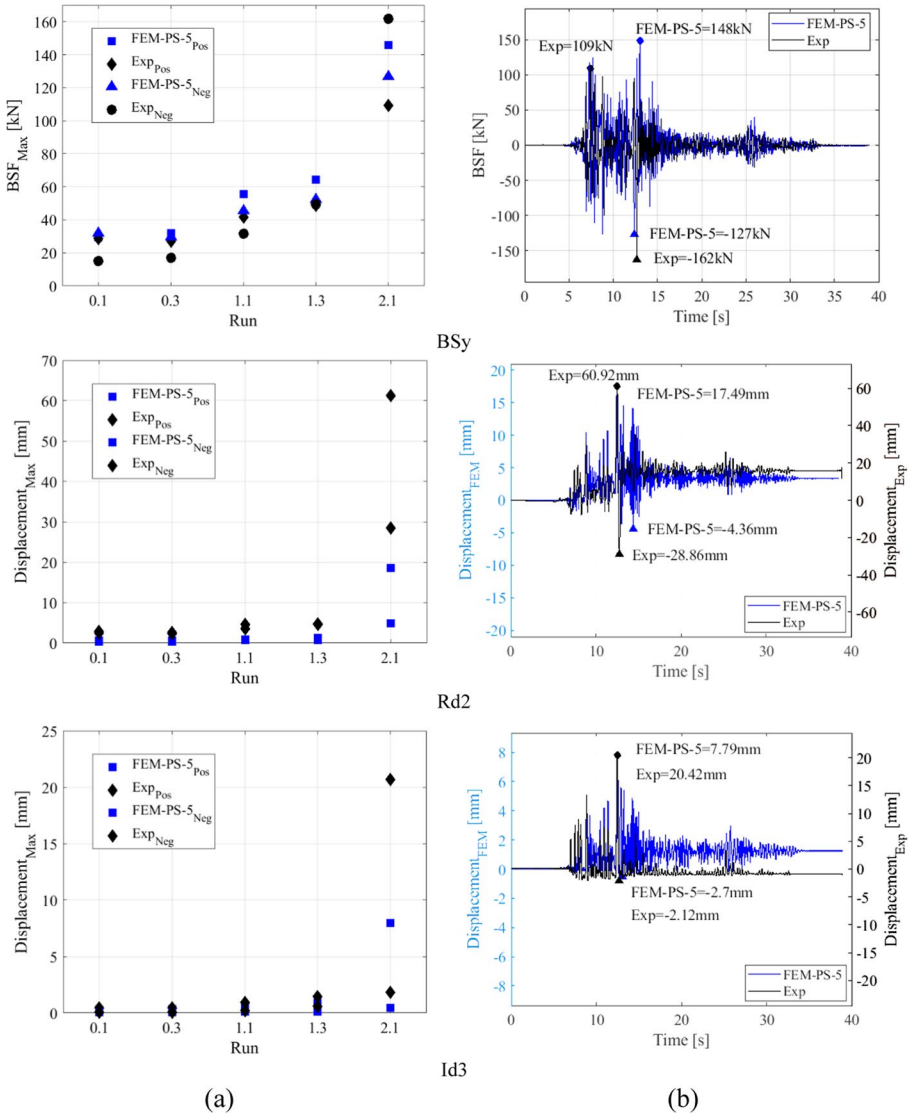


**Fig. 15** Comparison the experimental results and post-diction numerical results in terms of Bsy, Rd2 and Id3: **a** maximum values for each run; **b** time histories at Run 2.1

## 6 Conclusions

This work presents the pre- and post-diction numerical simulations carried on a two-unit stone masonry aggregate that was subjected to incremental dynamic testing within the SERA – AIM project. In the pre-diction study, two finite element models, FEM-4 and FEM-5, were developed using macro-modelling approach and accounting for both in-plane and out-of-plane responses. Indeed, two different strategies were tested for modelling timber floors poorly connected to walls. FEM-4 implemented timber beams with nonlinear



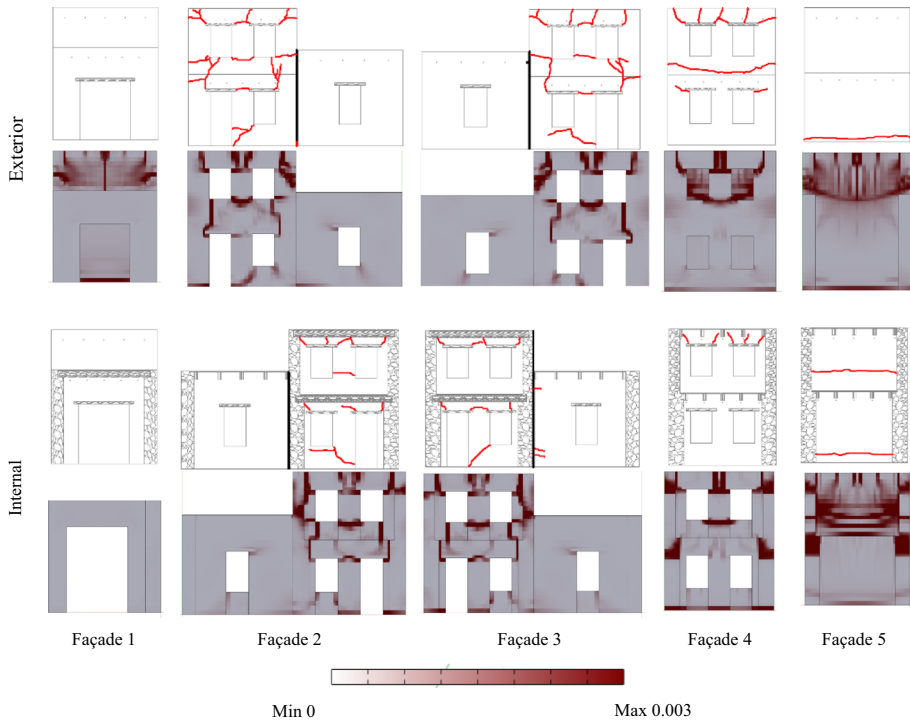


**Fig. 16** Comparison between the numerical post-diction results and the experimental results in terms of crack pattern (Run 2.1)

wall-to-floor connections, while FEM-5 did not model timber floors. Nonlinear incremental dynamic analysis showed that the models fairly estimated the experimental base shears (maximum error 30%), but they both underestimated the order of magnitude of displacements and predicted the crack pattern with considerable scatter. The nonlinear wall-to-floor connections implemented in FEM-4, even if calibrated for an unstrengthened configuration, still contributed to contrast out-of-plane failure mechanisms. Despite the limitations, FEM-5 resulted to be more suitable when compared with the test results. Thus, FEM-5 was selected for the post-diction, being updated into FEM-PS-5.

Based on the experimental data, major modifications in FEM-PS-5 interested a lower masonry Young's modulus value, and a calibrated impact behaviour for pounding of unit-to-unit connections. A more advanced and improved masonry material model by Petracca, Candeloro and Camata (2017a) is adopted, being more stable than the model proposed by Faria et al. (1998) and allowing hysteretic behaviour also in tension. Those modifications concurred to improve the response of the aggregate structure, in particular referring to failure modes and crack pattern. Indeed, FEM-PS-5 captured the flexural failure of piers and spandrels. In addition, the out-of-plane mechanisms were rather well simulated numerically, though with some differences in the crack pattern. The numerical model also well replicated pounding during the impact between the two units. However, overall FEM-PS-5 underestimated displacements.

The blind pre-diction contest confirmed how much the numerical results can be affected by the high level of uncertainties related with modelling assumptions for

masonry aggregate structures. Available experimental data resulted to play a crucial role, as highlighted in the post-diction phase. Still, the study pointed out the current challenge in accurately modelling the behaviour of existing masonry aggregate structures, particularly referring to:

- With regards to wall-to-floor connections, nonlinear interfaces were adopted and calibrated on past experimental tests of typical weak connections for historical buildings, which represents a novelty when compared to previous studies. Though the outcomes seemed to be promising, the calibrated interface remained in the elastic range in this case, not in agreement with the laboratory observations. Therefore, additional experimental data for wall-to-floor connections are required to further improve the simulation of such structural connection and develop appropriate modelling guidelines at building scale.
- Concerning the unit-to-unit connections, which still represent a major challenge while modelling masonry aggregates, the simulation of the pounding/impact phenomenon was fairly simulated in the post-diction model. This was possible due to the experimental evidence gained from the shaking table tests, which allowed to update its opening limit.
- Some inconsistency was found in the post-diction model being too stiff. Among other reasons, this can be attributed to: (i) some limits when using a masonry Young's modulus value obtained from material characterisation test at building scale, and (ii) structure-foundation interface. Dynamic identification tests providing the full dynamic properties of the structure can be useful to investigate these aspects in future works.

**Acknowledgements** The authors thank the research groups at EPFL, University of Pavia, RWTH Aachen and UC Berkeley, who organised the blind prediction contest and in particular Igor Tomić who continuously supported the team. The authors are grateful to the National Laboratory of Civil Engineering for providing the experimental data for the shake table tests. The authors also thank three reviewers, whose comments have contributed to significantly improve the quality of this manuscript.

**Author contributions** All authors contributed to the study conception, methodology and design; their workforce was addressed to the conception or design of the work; either referring to the analysis and interpretation of results. The first draft of the manuscript was written by NB and MPC. All authors commented on previous versions of the manuscript. All authors read and approved the final manuscript.

**Funding** Open access funding provided by FCTIFCCN (b-on). This work has been partly financed by FCT—Foundation for Science and Technology.

## Declarations

**Conflict of interests** The authors certify that they have no affiliations with or involvement in any organization or entity with any financial interest, or non-financial interest in the subject matter or materials discussed in this manuscript.

**Open Access** This article is licensed under a Creative Commons Attribution 4.0 International License, which permits use, sharing, adaptation, distribution and reproduction in any medium or format, as long as you give appropriate credit to the original author(s) and the source, provide a link to the Creative Commons licence, and indicate if changes were made. The images or other third party material in this article are included in the article's Creative Commons licence, unless indicated otherwise in a credit line to the material. If material is not included in the article's Creative Commons licence and your intended use is not permitted by statutory regulation or exceeds the permitted use, you will need to obtain permission directly from the copyright holder. To view a copy of this licence, visit <http://creativecommons.org/licenses/by/4.0/>.

## References

- Angelillo M (2014) Mechanics of masonry structures. vol. 551. <https://doi.org/10.1007/978-3-7091-1774-3>
- Arash E, Zaghi E, Cashany M (2014) ZeroLengthImpact3D. University of Connecticut. 2014
- Aşıkoğlu A, Graça V, Paulo BL, Bartolomeo P (2020) Pushover analysis of unreinforced irregular masonry buildings: lessons from different modeling approaches. *Eng Struct*. <https://doi.org/10.1016/j.engstruct.2020.110830>
- Benedetti D, Carydis PG, Pezzoli P (1998) Shaking table tests on 24 Simple masonry buildings. *Earthquake Eng Struct Dynam* 27(1):67–90
- Bruneau M (1994) State-of-the-art report on seismic performance of unreinforced masonry buildings. *J Struct Eng* 120(1):230–251. [https://doi.org/10.1061/\(ASCE\)0733-9445](https://doi.org/10.1061/(ASCE)0733-9445)
- Carocci C (2012) Small centres damaged by 2009 L'Aquila Earthquake: on site analyses of historical masonry aggregates. *Bull Earthq Eng* 10(1):45–71. <https://doi.org/10.1007/s10518-011-9284-0>
- Carvalho E (1998) Seismic testing structures. In: 11th European conference on earthquake engineering
- Casapulla C, Portioli F (2016) Experimental tests on the limit states of dry-jointed tuff blocks. *Mater Struct/materiaux Et Constr* 49(3):751–767. <https://doi.org/10.1617/s11527-015-0536-3>
- Castellazzi G, D'Altri AM, de Miranda S, Chiozzi A, Tralli A (2018) Numerical Insights on the seismic behavior of a non-isolated historical masonry tower. *Bull Earthq Eng* 16(2):933–961. <https://doi.org/10.1007/s10518-017-0231-6>
- CEN EN 338 (2016) EN 338:2016-Structural timber—Strength classes, issued 2016. <http://www.buildingconservation.com/articles/structural-timber-repairs/structural-timber-repairs.htm>
- CEN (2001) Eurocode 6: design of masonry structures. Design Studies, issued 2001
- Charney FA (2008) Unintended consequences of modeling damping in structures. *J Struct Eng* 134(4):581–592. [https://doi.org/10.1061/\(ASCE\)0733-9445\(2008\)134:4\(581\)](https://doi.org/10.1061/(ASCE)0733-9445(2008)134:4(581))
- Chopra AK (2012) Dynamics of structures. Theory and Applications to Earthquake Engineering. Englewood Cliffs: Prentice Hall
- Cioci MP, Sharma S, Lourenço PB (2018) Engineering simulations of a super-complex cultural heritage building: Ica cathedral in Peru. *Meccanica* 53(7):1931–1958. <https://doi.org/10.1007/s11012-017-0720-3>
- D'Altri AM, Milani G, De Miranda S, Castellazzi G, Sarhosis V (2018) Stability analysis of leaning historic masonry structures. *Autom Constr* 92:199–213
- D'Altri AM, Sarhosis V, Milani G, Rots JG, Cattari S, Lagomarsino S, Sacco E, Tralli A, Castellazzi G, de Miranda S (2019) Modeling strategies for the computational analysis of unreinforced masonry structures: review and classification. *Archives Comput Methods Eng*. <https://doi.org/10.1007/s11831-019-09351-x>
- D'Ayala DF, Sara P (2011) Assessment and analysis of damage in L' Aquila Historic city centre after 6th April 2009. *Bulletin Earthquake Eng*. <https://doi.org/10.1007/s10518-010-9224-4>
- Dizhur D, Ingham J, Moon LM, Griffith MC, Schultz A, Senaldi IE, Magenes G et al (2011) Performance of masonry buildings and churches in the 22 February 2011 Christchurch earthquake. *Bull N Z Soc Earthq Eng* 44(4):279–296
- Faria R, Oliver J, Cervera M (1998) A Strain-based plastic viscous-damage model for massive concrete structures. *Int J Solids Struct*. [https://doi.org/10.1016/S0020-7683\(97\)00119-4](https://doi.org/10.1016/S0020-7683(97)00119-4)
- Fenves GL (2014) ZeroLength Element. University of Texas, Austin, p 2014
- Giuffré A (1993) Sicurezza e Conservazione Dei Centri Storici. Rome, Italy: Laterza
- Guerrini G, Senaldi I, Graziotti F, Magenes G, Beyer K, Penna A (2019) Shake-table test of a strengthened stone masonry building aggregate with flexible diaphragms. *Int J Archit Heritage* 13(7):1078–1097. <https://doi.org/10.1080/15583058.2019.1635661>
- Guerrini G, Senaldi I, Scherini S, Morganti S, Magenes G, Beyer K, Penna A (2017) Material characterization for the shaking-table test of the scaled prototype of a stone masonry building aggregate. In: Proceedings of XVII Convegno ANIDIS “L'Ingegneria Sismica in Italia
- Hilber HM, Hughes TJR, Taylor RL (1977) Improved numerical dissipation for time integration algorithms in structural dynamics. *Earthquake Eng Struct Dynam* 5(3):283–292. <https://doi.org/10.1002/eqe.4290050306>
- Lourenço PB (2002) Computations on historic masonry structures. *Prog Struct Mat Eng* 4(3):301–319. <https://doi.org/10.1002/pse.120>
- Lourenço PB, Ramos LF (2004) Characterization of cyclic behavior of dry masonry joints. *J Struct Eng* 130(5):779–786. [https://doi.org/10.1061/\(ASCE\)0733-9445](https://doi.org/10.1061/(ASCE)0733-9445)
- Lourenço PB, Mendes N, Ramos LF, Vitorino de Castro Oliveira. D (2011) Analysis of masonry structures without box behavior. *Int J Archit Heritage* 5(4–5):369–382. <https://doi.org/10.1080/15583058.2010.528824>

- Love Edward, Sandia National Laboratories (2018) StdBrick: Standard Brick Element 2018
- Mazzon N, Chavez CM, Valluzzi MR, Casarin F, Modena C (2010) Shaking table tests on multi-leaf stone masonry structures: analysis of stiffness decay. *Adv Mater Res Trans Tech Publ* 133:647–652
- McKenna F, Fenves GL, Filippou FC, Scott M (2000) Open System for earthquake engineering simulation (OpenSees). University of California, Berkeley
- Mendes N, Lourenço PB (2010) Seismic assessment of masonry gaioleiro buildings in Lisbon, Portugal. *J Earthquake Eng* 14(1):80–101. <https://doi.org/10.1080/13632460902977474>
- Mendes N, Lourenço PB (2014) Sensitivity analysis of the seismic performance of existing masonry buildings. *Eng Struct* 80:137–146. <https://doi.org/10.1016/j.engstruct.2014.09.005>
- Ministero delle Infrastrutture e Trasporti (2019) Circolare esplicativa delle norme tecniche per le costruzioni, issued 2019.
- Moreira S (2015) Seismic retrofit of masonry-to-timber connections in historical constructions. Guimarães, Portugal: PhD Thesis, University of Minho
- Panella DS, Tornello ME, Frau CD (2017) A simple and intuitive procedure to identify pulse-like ground motions. *Soil Dyn Earthquake Eng* 94:234–43. <https://doi.org/10.1016/j.soildyn.2017.01.020>
- Papanikolaou VK, Kartalis-Kaounis T, Protopapadakis VK, Papadopoulos T (2017) GiD+OpenSees Interface: An Integrated Finite Element Analysis Platform. Lab of R/C and Masonry Structures, Aristotle University of Thessaloniki, Greece
- Parisse F, Cattari S, Marques R, Lourenço PB, Magenes G, Beyer K, Bruno Calderoni M, Karakaya DM, Manzini CF (2021) Benchmarking the seismic assessment of unreinforced masonry buildings from a blind prediction test. *Structures* 31:982–1005. <https://doi.org/10.1016/j.istruc.2021.01.096>
- Penna A, Morandi P, Rota M, Manzini CF, Da Porto F, Magenes G (2014) Performance of Masonry buildings during the emilia 2012 Earthquake. *Bulletin Earthquake Eng*. <https://doi.org/10.1007/s10518-013-9496-6>
- Petracca M, Pelà L, Rossi R, Zaghi S, Camata G, Spacone E (2017b) Micro-scale continuous and discrete numerical models for nonlinear analysis of masonry shear walls. *Constr Build Mater* 149:296–314. <https://doi.org/10.1016/j.conbuildmat.2017.05.130>
- Petracca M, Camata G (2019) A mixed implicit-explicit tension-compression plastic-damage model. Pescara, Italy: ASDEA Software Technology
- Petracca M, Candeloro M, Camata G (2017a) STKO user manual. Pescara, Italy: ASDEA Software Technology
- Puncello I, Caprili S, Roca P (2022) Simplified numerical approach for the structural analysis of monumental historical aggregates: the case study of certosa di calci. *Bull Earthq Eng*. <https://doi.org/10.1007/s10518-022-01397-w>
- Ramírez Álvarez de Lara R, Mendes N, Lourenço PB (2019) Diagnosis and seismic behavior evaluation of the church of são miguel de refojos (Portugal). *Buildings*. <https://doi.org/10.3390/BUILDINGS9060138>
- Roca P, Cervera M, Gariup G, Pelà L (2010) Structural analysis of masonry historical constructions. Classical and advanced approaches. *Archives Comput Methods Eng* 17(3):299–325. <https://doi.org/10.1007/s11831-010-9046-1>
- Saloustros S, Pelà L, Roca P (2020) Nonlinear numerical modeling of complex masonry heritage structures considering history-related phenomena in staged construction analysis and material uncertainty in seismic assessment. *J Perform Construc Facilities*. [https://doi.org/10.1061/\(ASCE\)CF.1943-5509.0001494](https://doi.org/10.1061/(ASCE)CF.1943-5509.0001494)
- Scott M, Filippou FC (2016) Hysteretic material model. Oregon State University, UC Berkeley, p 2016
- Senaldi IE, Magenes G, Penna A, Galasco A, Rota M (2014) The Effect of stiffened floor and roof diaphragms on the experimental seismic response of a full-scale unreinforced stone masonry building. *J Earthquake Eng* 18(3):407–443
- Senaldi IE, Guerrini G, Scherini S, Morganti S, Magenes G, Beyer K, Penna A (2018) Natural stone masonry characterization for the shaking-table test of a scaled building specimen. In: *Proceedings of the international masonry society conferences*, 0:1530–1545
- Solarino F, Vitorino de Castro Oliveira D, Giresini L (2019) Wall-to-horizontal diaphragm connections in historical buildings: a state-of-the-art review. *Eng Struct* 199:109559. <https://doi.org/10.1016/j.engstruct.2019.109559>
- Solarino F, Oliveira DV, Giresini L (2021) Numerical development of a strengthened wall-to-diaphragm seismic connection: calibration and application on a building prototype. In: *12th international conference on structural analysis of historical constructions (SAHC)* <https://doi.org/10.23967/sahc.2021.171>.
- Sorrentino L, Cattari S, da Porto F, Magenes G, Penna A (2019) Seismic behaviour of ordinary masonry buildings during the 2016 central Italy earthquakes. *Bull Earthq Eng* 17(10):5583–5607. <https://doi.org/10.1007/s10518-018-0370-4>

- Stepinac M, Lourenço PB, Atalić J, Kišiček T, Uroš M, Baniček M, Novak MŠ (2021) Damage classification of residential buildings in historical downtown after the ML55 earthquake in Zagreb, Croatia in 2020. *Int J Disaster Risk Reduct* 56:102140. <https://doi.org/10.1016/j.ijdrr.2021.102140>
- Tomažević M, Weiss P, Velechovsky T (1991) The influence of rigidity of floors on the seismic behaviour of old stone-masonry buildings. *European Earthquake Engineering*
- Tomažević M, Velechovsky T, Weiss P (1992) The effect of interventions in the floor structural system on the seismic resistance of historic stone-masonry buildings: an experimental study. In: 10th world conference on earthquake engineering. Madrid, Spain
- Tomažević M (1999) *Earthquake-Resistant Design of Masonry Buildings*. Edited by Imperial College Press. vol. 1. London: Imperial College Press
- Tomić I, Penna A, Dejong MJ (2022a) Shake table testing of a half-scale stone masonry building. *Bulletin Earthquake Eng*
- Tomić I, Penna A, Dejong MJ, Butenweg C, Correia A, Candeias PX, Senaldi IE (2022b) Shake-table testing of a stone masonry building aggregate: overview of blind prediction study. *Bulletin Earthquake Eng*
- Vasconcelos G, Lourenço PB, Vitorino de Castro Oliveira D (2008) Experimental shear behavior of stone masonry joints. In: Francesca D'Ayala D (ed) *Structural analysis of historical constructions*, pp 771–79. London: Taylor & Francis Group. <https://doi.org/10.1201/9781439828229.ch87>
- Vintzileou E, Mouzakis C, Adami CE, Karapitta L (2015) Seismic behavior of three-leaf stone masonry buildings before and after interventions: shaking table tests on a two-storey masonry model. *Bulletin Earthquake Eng* 13:3107–3133. <https://doi.org/10.1007/s10518-015-9746-x>

**Publisher's Note** Springer Nature remains neutral with regard to jurisdictional claims in published maps and institutional affiliations.